



Internal Note/
ALICE reference number

ALICE-INT-2011-XXX version 1.0

Date of last change: 30.05.2011

4 Comparison of hit-track matching efficiency with single-sided and
5 double-sided layers

6 **Authors:**

7 J. Baudot, S. Senyukov

8 *IPHC/ IN2P3-CNRS, Université de Strasbourg*

9 **Abstract**

10 The technology of CMOS pixel sensors, or MAPS, is offering a new optimiza-
11 tion between pixel granularity, readout speed, power dissipation and material
12 budget compared to technologies employed so far in high energy physics experi-
13 ments. Consequently, new approaches are emerging to integrate such detectors.
14 One of them consists in building double-sided detection layers which provide two
15 real-2D points whereas standard single-sided layers provides only one.

16 In this note, we explore the potential benefits of such double-sided layers for the
17 specific problem of associating hits with tracks. Indeed, large experiments usu-
18 ally dedicate separate sub-detectors for the *tracking* and the *vertexing*. In such
19 a case, reconstructed tracks need to be matched with their corresponding hits in
20 the, usually discrete, layers of the vertex detector. The efficiency of this matching
21 step for a given layer depends on the hit density, the uncertainty on the track
22 parameters at this layer -wich embeds the geometry and spatial resolution of the
23 previous layers- and, of course, on the spatial accuracy of the layer itself.

1 Introduction

An essential step of any tracking algorithm consists in associating hits together to form a track. In this note, we consider the specific case of the association of hits measured in a vertex detector, with tracks that have been already reconstructed by a tracker surrounding the vertex detector. This is the typical case of experiments like STAR, ALICE or ILD where tracking proceeds in two steps. Firstly, a time projection chamber (TPC) allows to individualize tracks. Then those tracks are extrapolated toward the primary collision vertex with the help of several inner layers. The extrapolation goes from one layer to the other, starting at the largest radius. The hit associated at each layer is used to update the track parameters. The track extrapolation accuracy toward the next layer increases with decreasing radius which helps to fight against the increasing hit density.

For the purpose of optimizing the design of new detectors, it is extremely useful to predict the efficiency of the hit-track association for a given detector configuration. We define the matching efficiency at a given layer as the probability to associate the track reconstructed for a particle trajectory to the hit generated by this same particle in the layer.

One source of inefficiency is due to the detection efficiency ϵ_{det} of the layer not being 100 %. If considering a double-sided layer the probability to get at least one measurement point is $(1 - (1 - \epsilon_{det})^2)$ to be compared to ϵ_{det} for a single-sided layer. The gain obtained with the double-sided layer quantifies to $\epsilon_{det} \times (1 - \epsilon_{det})$ which is about 2% and 5% for $\epsilon_{det} = 98\%$ and 95% respectively. We shall not discuss further this point.

The other part of the inefficiency for matching a track with the corresponding hit stems from the presence on the layer of other hits than the one looked for. One easily understands that, if the hit is searched for in a given area, the probability depends on the hit density, the surface of the search area, the accuracy of the hit location and the criteria to select a hit. The exact expression for single-sided layers was derived analytically in [1] in the framework of the STAR Heavy Flavor Tracker design [2] study.

This work generalizes the computation of the matching efficiency for a double-sided layer. Such a layer provides two independent measurements with a radii difference of about 2 mm [3]. This set of two points allows to estimate the direction of the propagating track and not only its position at the layer radius. It is expected that the additional constraint improves the matching efficiency. However, the number of so-called mini-vectors built from the combination of any of the hits present on the two sides of the layer increases like the square of the hit density. This fact tends to decrease the probability to match the correct hit. In other words, the single-sided case corresponds to a two dimensional problem

66 whereas the double-sided case is a problem in four dimensions. Our goal is to
 67 investigate in which domain of the parameter space the double-sided approach
 68 is beneficial or detrimental.

69
 70 The next section establishes the probability expression in the general case,
 71 then comparative results for the single-sided and double-sided layer cases are
 72 discussed in the last section.

73 2 General formula for the matching efficiency

74 2.1 Matching procedure

75 Before deriving a formula for the efficiency, we shall describe the matching
 76 procedure. It is based on the χ^2 approach as introduced in [1].

77 We define the typical collider geometry where the z axis is parallel to the beam
 78 axis and the $R\phi$ plane is perpendicular to it. We localize a point in the local
 79 planar geometry of a given layer at a radius r with the coordinates (x, z) where
 80 the x axis is perpendicular to the beam and the radius.

81
 82 A track, with a given direction is extrapolated inward on a layer at a known
 83 radius (r) with a pointing accuracy $\sigma_{ext,R\phi}(r)$ in the transverse plane and $\sigma_{ext,z}(r)$
 84 along the beam axis. The layer itself features an intrinsic spatial resolution in
 85 both directions respectively $\sigma_{int,R\phi}(r)$ and $\sigma_{int,z}(r)$. The following χ^2 provides a
 86 quantitative estimation of the matching quality between the track extrapolation
 87 crossing the layer at x_t, z_t and a hit located at position x_p, z_p on this layer:

$$\chi^2(x_p, z_p) = \frac{(x_t - x_p)^2}{\sigma_{\text{eff},R\phi}^2} + \frac{(z_t - z_p)^2}{\sigma_{\text{eff},z}^2}. \quad (1)$$

88 The standard deviations used in the previous equation are defined as the
 89 quadratic sum of the extrapolated and intrinsic spatial resolution in both
 90 directions: $\sigma_{\text{eff}}^2 = \sigma_{ext}^2 + \sigma_{int}^2$. Usually $\sigma_{ext} \gg \sigma_{int}$, so we denote the overall σ_{eff}
 91 as an effective spatial resolution in the following. The hit with the lowest χ^2 is
 92 chosen for the association.

93
 94 When matching simultaneously two layers at different radii r_1 and r_2 , the
 95 χ^2 properties authorize a simple sum of both χ^2 corresponding to a couple of
 96 points $((x_{1,p}, z_{1,p}), (x_{2,p}, z_{2,p}))$ associated with effective uncertainties for each layer,
 97 respectively $((\sigma_{\text{eff}1,R\phi}, \sigma_{\text{eff}1,z}), (\sigma_{\text{eff}2,R\phi}, \sigma_{\text{eff}2,z}))$:

$$\chi^2(x_{1,p}, z_{1,p}, x_{2,p}, z_{2,p}) = \frac{(x_{1,t} - x_{1,p})^2}{\sigma_{\text{eff}1,R\phi}^2} + \frac{(z_{1,t} - z_{1,p})^2}{\sigma_{\text{eff}1,z}^2} + \frac{(x_{2,t} - x_{2,p})^2}{\sigma_{\text{eff}2,R\phi}^2} + \frac{(z_{2,t} - z_{2,p})^2}{\sigma_{\text{eff}2,z}^2}. \quad (2)$$

98 The mini-vector, which can be built out of the two points, does not appear
 99 explicitly in the previous equation. Indeed, no angle is computed that can be
 100 compared to the track parameters. However, equation 2 implicitly contains this
 101 comparison since the track projections in both layers $((x_{1,t}, z_{1,t}), (x_{2,t}, z_{2,t}))$ and
 102 their uncertainties are taken into account simultaneously. This approach also
 103 copes naturally with non-straight tracks.

104

105 We observe that the χ^2 dimension, or number of parameters, increases from
 106 2 with a single-sided layer to 4 with a double-sided layer. Generalizing, trying
 107 to match n 2D measurements simultaneously would lead to a $2n$ dimensional
 108 problems. Mathematically the matrix formalism is best suited to deal with any
 109 number of dimensions. So we define the following $2n$ -vector and $2n \times 2n$ -matrix:

$$\vec{X} = [x_{1,t} - x_{1,p}, z_{1,t} - z_{1,p}, \dots, x_{n,t} - x_{n,p}, z_{n,t} - z_{n,p}], \quad (3)$$

$$\Sigma^{-1} = \begin{pmatrix} \frac{1}{\sigma_{\text{eff}1,\text{R}\phi}^2} & 0 & \dots & 0 & 0 \\ 0 & \frac{1}{\sigma_{\text{eff}1,z}^2} & \dots & 0 & 0 \\ \dots & \dots & \dots & \dots & \dots \\ 0 & 0 & \dots & \frac{1}{\sigma_{\text{eff}n,\text{R}\phi}^2} & 0 \\ 0 & 0 & \dots & 0 & \frac{1}{\sigma_{\text{eff}n,z}^2} \end{pmatrix}. \quad (4)$$

110 The vector \vec{X} contains the two coordinates of each 2D vector joining a hit and
 111 the track on a given side. The weight matrix Σ^{-1} is the usual inverse of the
 112 covariance matrix which allows to obtain the general χ^2 expression:

$$\chi^2(\vec{X}) = \vec{X}^T \Sigma^{-1} \vec{X}. \quad (5)$$

113 The set of n hits related to the track is searched as the one with the minimal
 114 χ^2 of all the sets of n hits located in a $2n$ -volume (noted V_{2n} in the following)
 115 centered on the track extrapolation and extended in each dimension by $\pm f \times \sigma_{\text{eff}}$
 116 where f is usually above 3. Indeed, lower values of f would limit the matching
 117 efficiency due to an insufficient search area.

118 2.2 Computing the matching efficiency

119 Computing the matching efficiency is equivalent to the estimation of the proba-
 120 bility $P_{n,\text{match}}$ that the real set of n hits generated by the particle is present in
 121 the searched $2n$ -volume V_{2n} and has the minimal χ^2 of all the sets of n hits in
 122 this volume. The latter writes as an $2n$ -dimensional integral over the volume V_{2n}

$$P_{n,\text{match}} = \int_{V_{2n}} P_{nh}(\vec{X}) \times \frac{dP_h(\vec{X})}{d\vec{X}} d^{2n} \vec{X}, \quad (6)$$

123 where

- 124 • $\frac{dP_h(\vec{X})}{d\vec{X}} d^{2n}\vec{X}$ is the probability that the true set of hits generated by the
- 125 particle is located in an elementary volume $d\vec{X}$ around the position \vec{X} ,
- 126 • $P_{nh}(\vec{X})$ is the probability that no other set of n hits has a χ^2 lower than
- 127 the true hit.

128 The probability density that the correct set of n hits lies at the position \vec{X} is
 129 simply a $2n$ -dimensional normal distribution:

$$\frac{dP_h(\vec{X})}{d\vec{X}} = \frac{1}{(2\pi)^{n/2}\sqrt{\det\Sigma}} \exp\left[-\frac{1}{2}\vec{X}^T\Sigma^{-1}\vec{X}\right] \quad (7)$$

130

131

132 The probability $P_{nh}(\vec{X})$ that no other set of n hits has a lower χ^2 than a fixed
 133 limit is given by the value of the Poisson distribution evaluated at 0, $\exp(-\nu_h(\vec{X}))$,
 134 where the expected number of hit sets $\nu_h(\vec{X})$ corresponds to the average number
 135 of n -tuplets of hits with a χ^2 lower than the limit defined by $\chi^2(\vec{X})$.

136 In order to estimate this average number $\nu_h(\vec{X})$ we would need to know the
 137 distribution of the hits on the different measurement layers and their correlation.
 138 To simplify our computation we assume those hit distributions to be uncorrelated,
 139 uniform in 2D and equal to ρ^1 . The no-correlation hypothesis is not realistic
 140 because hits are generated by tracks. However it certainly represents a worst
 141 case and leads to uniform density ρ^n in the $2n$ -dimensional space generated by
 142 the n measurements.

143 Because of this uniformity, the average number of hits, $\nu_h(\vec{X})$ is the density of hits
 144 in $2n$ D multiplied by the $2n$ -volume $E_{2n}(\vec{X})$ defining all the points \vec{X}_p verifying
 145 the inequality:

$$\chi^2(\vec{X}_p) < \chi^2(\vec{X}), \quad (8)$$

$$\vec{X}_p^T \Sigma^{-1} \vec{X}_p < \vec{X}^T \Sigma^{-1} \vec{X}, \quad (9)$$

$$\vec{X}_p^T \frac{\Sigma^{-1}}{\vec{X}^T \Sigma^{-1} \vec{X}} \vec{X}_p < 1. \quad (10)$$

146 The latter form defines an ellipsoid in $2n$ dimensions which volume $E_{2n}(\vec{X})$ is
 147 given by:

$$E_{2n}(\vec{X}) = \frac{\pi^n}{\Gamma(1+n)} \sqrt{\det \frac{\Sigma^{-1}}{\vec{X}^T \Sigma^{-1} \vec{X}}}, \quad (11)$$

$$E_{2n}(\vec{X}) = \frac{\pi^n}{\Gamma(1+n)} (\vec{X}^T \Sigma^{-1} \vec{X})^n \sqrt{\det \Sigma}. \quad (12)$$

¹Here, we assume that the hit density does not change from one side of the layer to the other side because the layer thickness is small enough (one or two millimeters).

148 So we get

$$\nu_h(\vec{X}) = \rho^n \times E_{2n}(\vec{X}), \quad (13)$$

149 and finally

$$P_{nh}(\vec{X}) = \exp\left[-\rho^n \frac{\pi^n}{\Gamma(1+n)} (\vec{X}^T \Sigma^{-1} \vec{X})^n \sqrt{\det \Sigma}\right]. \quad (14)$$

150 We can find the general expression of the matching efficiency or probability
151 $P_{n,match}$ in the following integral form:

$$P_{n,match} = \frac{1}{(2\pi)^n \sqrt{\det \Sigma}} \times \int_{2nD\text{-area}} d\vec{X} \exp\left[-\rho^n \frac{\pi^n}{\Gamma(1+n)} (\vec{X}^T \Sigma^{-1} \vec{X})^n \sqrt{\det \Sigma} - \frac{1}{2} \vec{X}^T \Sigma^{-1} \vec{X}\right]. \quad (15)$$

152 2.3 Expression for a single-sided layer

153 For a single-sided layer, we have a 2 dimensional problem, $n = 1$ for which
154 $\Gamma(1+n) = 1$, $\sqrt{\det \Sigma} = \sigma_{\text{effR}\phi} \sigma_{\text{effz}}$ and the search volume V_{2n} is simply a rectangle
155 of size $2f\sigma_{\text{effR}\phi} \times 2f\sigma_{\text{effz}}$. Thus, the formula 15 can be computed as:

$$P_{1,match} = \int_{-f\sigma_{\text{effR}\phi}}^{f\sigma_{\text{effR}\phi}} dx \int_{-f\sigma_{\text{effz}}}^{f\sigma_{\text{effz}}} dz \frac{1}{2\pi\sigma_{\text{effR}\phi}\sigma_{\text{effz}}} \times \exp\left[-\rho\pi\sigma_{\text{effR}\phi}\sigma_{\text{effz}}\vec{X}^T \Sigma^{-1} \vec{X} - \frac{1}{2}\vec{X}^T \Sigma^{-1} \vec{X}\right], \quad (16)$$

$$P_{1,match} = \int_{-f\sigma_{\text{effR}\phi}}^{f\sigma_{\text{effR}\phi}} \exp\left[-(2\rho\pi\sigma_{\text{effR}\phi}\sigma_{\text{effz}} + 1)\frac{x^2}{2\sigma_{R\phi}^2}\right] dx \times \int_{-f\sigma_{\text{effz}}}^{f\sigma_{\text{effz}}} \exp\left[-(2\rho\pi\sigma_{\text{effR}\phi}\sigma_{\text{effz}} + 1)\frac{z^2}{2\sigma_z^2}\right] dz, \quad (17)$$

$$P_{1,match} = \frac{\text{erf}^2\left(f\sqrt{\frac{1+2\pi\sigma_{\text{effR}\phi}\sigma_{\text{effz}}\rho}{2}}\right)}{1 + 2\pi\sigma_{\text{effR}\phi}\sigma_{\text{effz}}\rho}. \quad (18)$$

156 These results were already obtained in [1]. If the search area is sufficiently large,
157 $f \gg 3$, the error function can be approximated by 1 and we get the infinite search
158 area efficiency:

$$P_{1,match} = \frac{1}{1 + 2\pi\sigma_{\text{effR}\phi}\sigma_{\text{effz}}\rho}. \quad (19)$$

159 This equation clearly demonstrates that, in the single-sided case, the figure of
160 merit for the matching efficiency is the product $\sigma_{\text{effR}\phi}\sigma_{\text{effz}}\rho$ where each term, the
161 two effective resolutions and the density, contribute equally to the power of 1.
162 We also infer from equation 19 that lines with constant probability $P_{1,match}$ are
163 hyperbolae in the planes $(\sigma_{\text{effR}\phi}, \sigma_{\text{effz}})$ or (σ, ρ) .

164 2.4 Expression for a double-sided layer

165 For a double-sided layer, we have a 4 dimensional problem, $n = 2$ for which
 166 $\Gamma(1 + n) = 2$, $\sqrt{\det\Sigma} = \sigma_{\text{eff}1,\text{R}\phi}\sigma_{\text{eff}1,\text{z}} \times \sigma_{\text{eff}2,\text{R}\phi}\sigma_{\text{eff}2,\text{z}}$ and the search volume V_{2n} is
 167 a 4D rectangle. Thus, the formula 15 can be computed as:

$$P_{2,\text{match}} = \frac{1}{(2\pi)^2\sigma_{\text{eff}1,\text{R}\phi}\sigma_{\text{eff}1,\text{z}}\sigma_{\text{eff}2,\text{R}\phi}\sigma_{\text{eff}2,\text{z}}} \int_{-fx_1}^{fx_1} \int_{-fz_1}^{fz_1} \int_{-fx_2}^{fx_2} \int_{-fz_2}^{fz_2} dx_1 dz_1 dx_2 dz_2$$

$$\exp\left[-\frac{\pi^2}{2}(\vec{X}^T\Sigma^{-1}\vec{X})^2 \rho^2 \sigma_{\text{eff}1,\text{R}\phi}\sigma_{\text{eff}1,\text{z}}\sigma_{\text{eff}2,\text{R}\phi}\sigma_{\text{eff}2,\text{z}} - \frac{1}{2}\vec{X}^T\Sigma^{-1}\vec{X}\right]. \quad (20)$$

168 Contrary to the 2D case (single measurement), a second order term
 169 $(\vec{X}^T\Sigma^{-1}\vec{X})^2$ appears which prevents the easy breakdown of the 4D integral into
 170 a product of four 1D integrals. Thus, we relied on a numerical computation
 171 (Monte-Carlo integration) in this case. Similarly we observe that the density ρ
 172 appears at the power of 2 in the formula.

173 3 Results

174 In this section, we present computation results in order to compare the two
 175 layer types: single-sided and double-sided. We remind the reader that we have
 176 assumed the hit distribution to be uncorrelated on both sides of the double-sided
 177 layer case. Our results shall then be taken as the worst matching efficiency for
 178 the latter.

179 As depicted in the introduction, the two sides of the double layer case are
 180 spaced only by a millimeter or two, so that we can approximate that the
 181 extrapolation of the track has the same accuracy on both sides. We also consider
 182 that the measurements on the two sides have the same uncertainty so that
 183 $\sigma_{\text{eff}1,\text{R}\phi} \approx \sigma_{\text{eff}2,\text{R}\phi} = \sigma_{\text{effR}\phi}$ and $\sigma_{\text{eff}1,\text{z}} \approx \sigma_{\text{eff}2,\text{z}} = \sigma_{\text{effz}}$. Consequently, for both
 184 cases, single-sided or double-sided, there are only three parameters on which the
 185 matching efficiency depends: the hit density ρ and the two resolutions $\sigma_{\text{effR}\phi}$ and
 186 σ_{effz} . In order to represent graphically the 3D function $P_{n,\text{match}}(\rho, \sigma_{\text{effR}\phi}, \sigma_{\text{effz}})$ we
 187 will use 1D and 2D plots with respectively two or one parameters fixed and 3D
 188 surfaces of fixed probability.

189
 190 For a first glimpse of the behavior of the matching efficiency we start with
 191 plotting in figure 1 the efficiency only with respect to the resolution σ_{effz} for a
 192 fixed hit density ρ and resolution $\sigma_{\text{effR}\phi}$. While the superiority of the double-sided
 193 approach is clearly observable in most of the represented conditions, a limit in hit
 194 density and effective resolution seems to appear, beyond which, the single-sided
 195 layer offers a better matching efficiency.

196

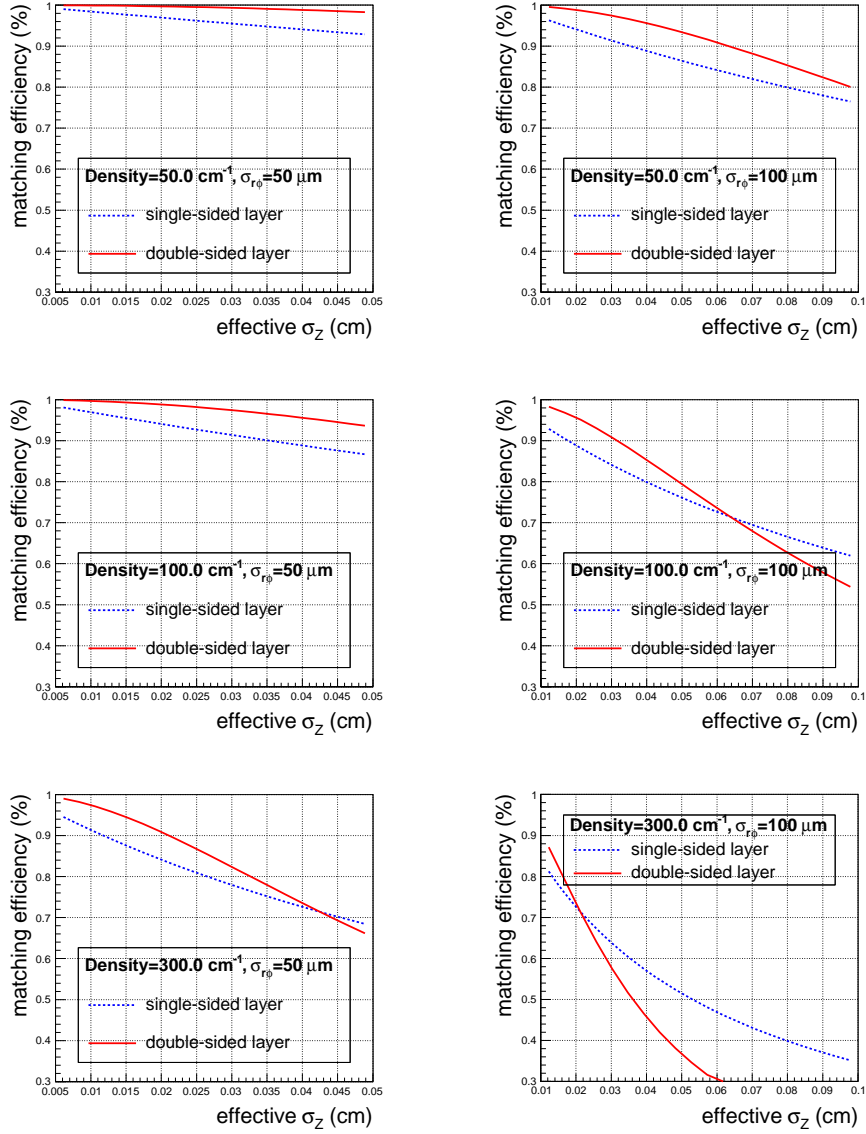


Figure 1: The matching efficiencies with respect to the effective resolution in z for a hit density varying from 50 to 300 particles/cm² and an effective resolution in $R\phi$ varying from 50 to 100 μ m; in red solid for the double-sided layer case and in blue dashed line for the single-sided layer case.

197 To gain a better insight on this limit, the efficiency difference is computed
 198 with respect to the effective resolutions in the two directions ($R\phi$ and z) for
 199 two fixed hit densities 90 and 300 particles/cm², see respectively figures 2 and 3
 200 where both resolutions are varied from 50 to 500 μm . Our choice of these ranges
 201 of parameters, is driven by the ALICE case [4]. The expected hyperbolic shape
 202 for constant matching efficiency lines is observed for the single-sided layer. The
 203 matching efficiency for the double-sided case exhibits a similar behavior but with
 204 a different curvature due to the higher order terms present in formula 20.
 205 Thus the area for the double-sided layer, where the matching efficiency stays
 206 above² 90 %, extends to worst effective resolutions by 100 μm or in some places
 207 by 200 μm . Although the absolute gain in matching efficiency never exceeds
 208 about 5 % in favour of the double-sided geometry, the extension of the 90 %
 209 efficiency domain by $\mathcal{O}(100 \mu\text{m})$ is particularly relevant for the overall tracking
 210 performance.
 211 Beyond some limits, the single-sided layer reaches better matching efficiency
 212 (with absolute difference exceeding 15 %) but this domain corresponds to rather
 213 marginal matching efficiency values, below 60 %. On the other hand, whenever
 214 the effective resolutions are excellent, below 80 μm for 90 particles/cm² or 50 μm
 215 for 300 particles/cm², in both directions ($R\phi$ and z), the two geometries display
 216 no difference in efficiency.

217 We explore further the impact of the hit density by fixing the ratio between
 218 the two effective resolutions $\sigma_{\text{eff}z}/\sigma_{\text{eff}R\phi}$ to 1 or 3 and plotting the matching
 219 efficiency versus the hit density ρ and resolution $\sigma_{\text{eff}R\phi}$ in figures 4 and 5. All
 220 our previous observations hold with these new curves.

221 When the conditions correspond to low hit densities combined with excellent
 222 effective resolution, the two geometries provide similar results. Performances of
 223 the two geometries depart whenever either the effective resolution or the density
 224 gets worse. The double-sided layer extends the domain where the matching
 225 efficiency stays above a given threshold. This is illustrated in the table 1 which
 226 lists the maximum densities allowed to reach significant matching efficiency
 227 thresholds with fixed effective pointing resolution conditions. We note again
 228 that the single-sided layer exhibits a better efficiency only when the absolute
 229 efficiency is quite low.

230

231 A final comparison between the two layer architectures is made through the
 232 display of the surface, in the 3D space $(\rho, \sigma_{\text{eff}R\phi}, \sigma_{\text{eff}z})$, corresponding to a fixed
 233 matching probability, see figure 6. Any point below the surface corresponds to an
 234 efficiency above the limit. The plot clearly demonstrates how much the double-
 235 sided layer extends the satisfactory operation domain.

²This is of course an arbitrary threshold, nevertheless considering lower matching efficiency seems of little interest.

Efficiency	Effective resolution (μm)		Maximum hit density (cm^{-2})	
	$R\phi$	z	Single	Double
90%	50	50	705	1265
	50	150	235	425
95%	50	50	335	860
	50	150	110	285
98%	50	50	130	530
	50	150	45	175
99%	50	50	65	370
	50	150	20	125

Table 1: Comparison of maximum hit densities (provided with a $\pm 5 \text{ cm}^{-2}$ uncertainty) to reach the 90, 95, 98 and 99 % matching efficiency levels with some fixed effective pointing resolutions in both directions for the single-sided layer and the double-sided layer.

4 Conclusion

In this note, we have followed an approach proposed in [1] to derive a general formula for the efficiency to match a track extrapolated to a detection layer with its corresponding hit. We have specifically explored the case of a double-sided layer which provides two equivalent measurements points separated only by one or two millimeters. We have computed the efficiency when the two measurements are considered simultaneously to better constrain the matching, under the assumption that the distribution of the hits on both layers are uncorrelated. This hypothesis certainly decreases the efficiency and hence our computation has to be considered as a worst case for the double-sided layer case. A future work based on a Monte-Carlo simulation will evaluate the impact of our assumption. Within this approach the matching is done with the hit presenting the best χ^2 , computed from the quadratic sum of ratios of the hit to track distance in some direction over a resolution which combines the layer spatial accuracy and the tracking extrapolation uncertainty on that layer. We found that the matching efficiency depends on an equal footing on three prominent parameters: the hit density on the layer and the two resolutions in the detection plane. From 2D graphical representations of the matching efficiency we separated the parameter space in three domains.

When all parameters are favorable, i.e. low hit density and excellent spatial accuracy, the double-sided layer and single-sided layer present equivalently good efficiency close to 100 %. When at least two parameters are disadvantageous for the matching, the efficiency for both geometries drops severely down, though the single-sided layer matches the correct hit more often. This last observa-

261 tion partly stems from our simplifying hypothesis that the hit distributions
262 are independent for the two measurements of the double-sided case. In the
263 intermediate situation where only one of the three parameters makes the match-
264 ing difficult, the double-sided layer always exhibits better results for the efficiency.

265

266 The study shows that the double-sided layer allows to maintain good
267 matching-efficiency (above 90 %), in comparison to the single-layer approach,
268 in cases where either the hit density or the track pointing uncertainty in one of
269 the two directions is getting large. In other cases, when both parameters are
270 degraded, two solutions can be employed. The first one consists in decreasing
271 the integration time of the layer to lower the hit density; it is the traditional
272 way. Our computation clearly demonstrates that there is another way, as effi-
273 cient, consisting in improving the spatial resolution of the outer layers in order
274 to decrease the track extrapolation uncertainty on the present layer.

275 References

- 276 [1] H. Wieman, V. Perevoztchikov, <http://rnc.lbl.gov/~wieman/HitFinding2DXsq.htm>.
- 277 [2] Z. Xu *et al.*, *A heavy flavor tracker for STAR*, LBNL-PUB-5509, Mar 7,
278 2006.
- 279 [3] N. Chon-Sen *et al.*, *Development of ultra-light pixelated ladders for an ILC*
280 *vertex detector*, in proceedings of the 2010 International Linear Collider
281 Workshop (LCWS10 and LC10), Beijing, 26-30 March 2010.
- 282 [4] R. Turrisi, *ALICE pixel detector operations and performance* in proceedings
283 of *VERTEX 2010*, Proc. of Sci. (VERTEX 2010)007.

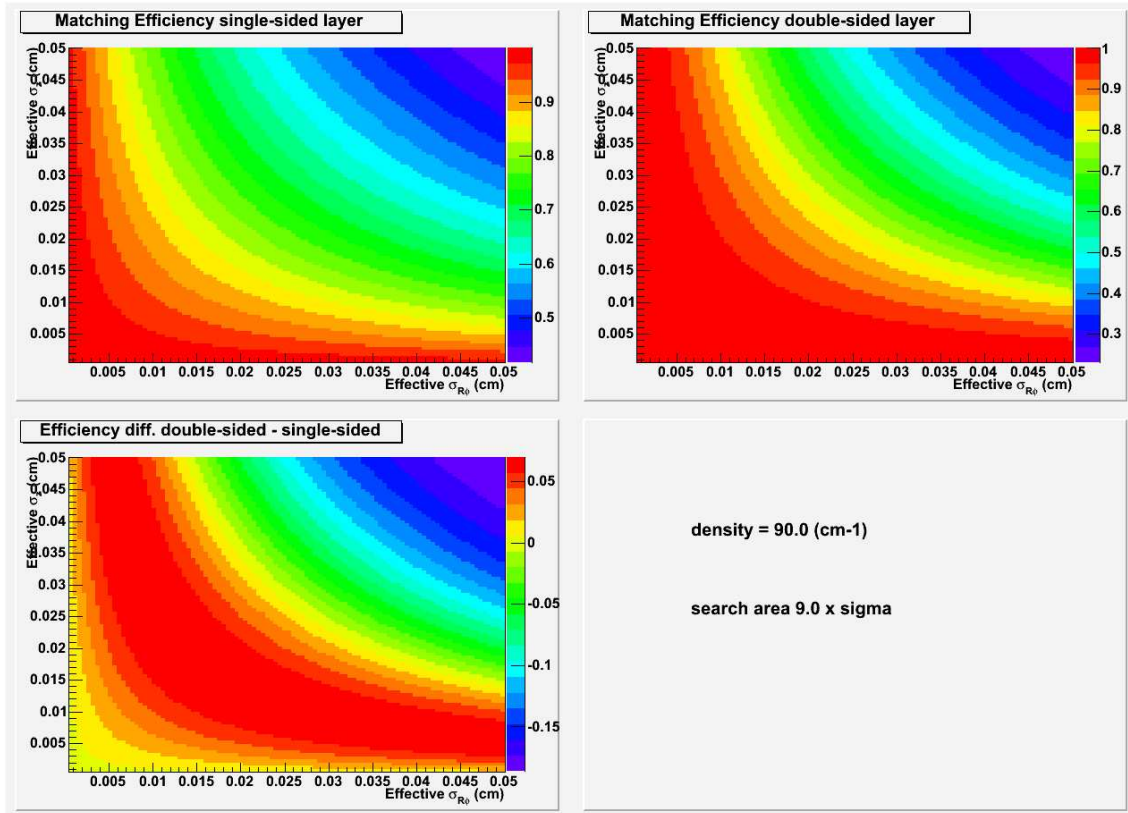


Figure 2: Top left plot shows the matching efficiency for a single-sided layer as a function of the effective resolutions in $R\phi$ and z for a fixed hit density of 90 particles/cm². Top right plot shows the same quantity but for a double-sided layer. Bottom plot shows the difference between the efficiencies for the double-sided and single-sided layers.

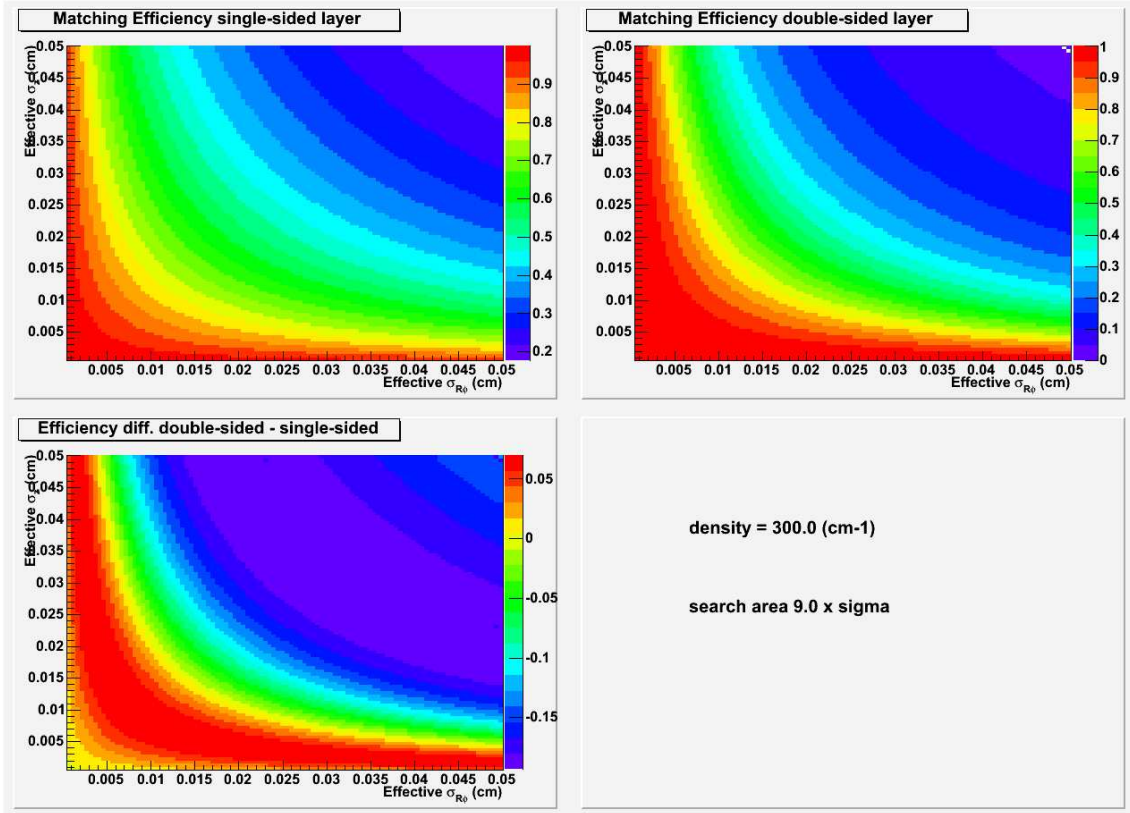


Figure 3: Top left plot shows the matching efficiency for a single-sided layer as a function of the effective resolutions in $R\phi$ and z for a fixed hit density of 300 particles/cm². Top right plot shows the same quantity but for a double-sided layer. Bottom plot shows the difference between the efficiencies for the double-sided and single-sided layers.

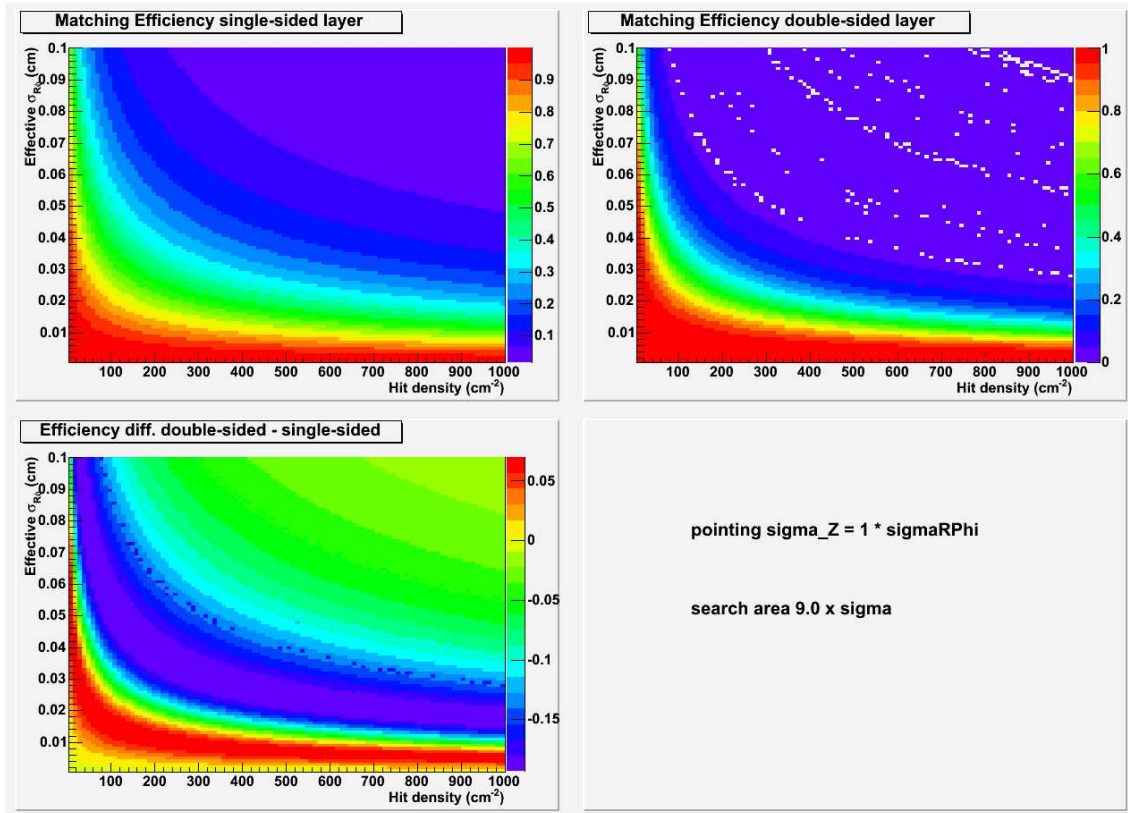


Figure 4: Top left plot shows the matching efficiency for a single-sided layer as a function of the hit density and the effective resolution in $R\phi$ for a fixed ratio $\sigma_{\text{effZ}}/\sigma_{\text{effR}\phi} = 1$. Top right plot shows the same quantity but for a double-sided layer. Bottom plot shows the difference between the efficiencies for the double-sided and single-sided layers.

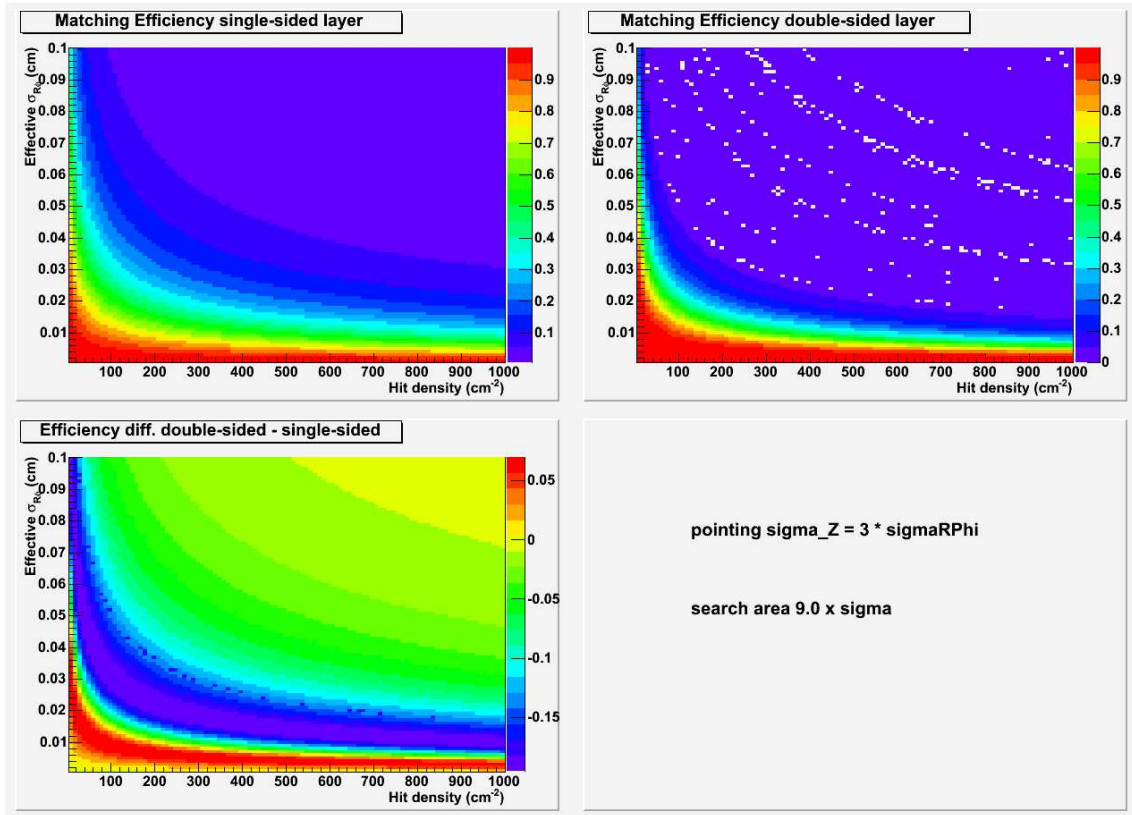


Figure 5: Top left plot shows the matching efficiency for a single-sided layer as a function of the hit density and the effective resolution in $R\phi$ for a fixed ratio $\sigma_{\text{eff}Z}/\sigma_{\text{eff}R\phi} = 3$. Top right plot shows the same quantity but for a double-sided layer. Bottom plot shows the difference between the efficiencies for the double-sided and single-sided layers.

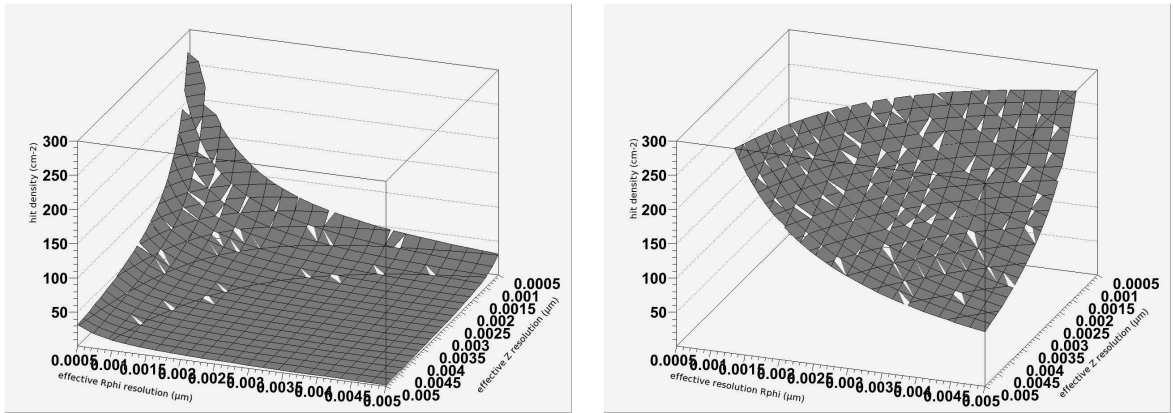


Figure 6: Surface of constant matching efficiency, here 99.95 %, for a single-sided layer on the left and for a double-sided layer on the right as a function of the effective resolutions in $R\phi$ and in z , and the hit density.